Phase Angle Feed-Forward Control for Improving the Power Reference Tracking of Virtual Synchronous Machines

Salvatore D'Arco and Jon Are Suul, *Member IEEE*

***Abstract*—A method for improving the power reference tracking capability of Virtual Synchronous Machines (VSM) by phase angle feed-forward (PAFF) control is proposed in this paper. The presented implementation includes compensation for the ac power flow dynamics and can be applied to any VSM-based control relying on a virtual swing equation. Fast and accurate power reference tracking is achieved independently from the emulated inertia time constant, and without influencing the grid synchronization mechanism of the VSM. Therefore, the grid forming capability of the VSM and the inertial response to grid frequency variations are not influenced by the proposed PAFF control. The effectiveness of the derived feed-forward terms is first validated with a simplified VSM scheme. The performance is also thoroughly evaluated for a detailed VSM implementation including closed loop current control and a virtual impedance. This includes operation with different grid impedance values and studies of the sensitivity of the PAFF function with respect to parameter variations in the VSM control or deviations from the assumed grid impedance. Experimental results with a 50 kVA converter controlled as a VSM are presented as verification of the improvement in power reference tracking capability.**

Keywords—Feed-forward, Grid Forming Control, Inertia Emulation, Virtual Synchronous Machines

I. Introduction

The control of Voltage Source Converters (VSCs) as Virtual Synchronous Machines (VSMs) has been extensively studied as an approach for providing virtual inertia and "grid-forming" functionality in modern power systems with declining inertia [1], [2]. Thus, a wide range of VSM implementations have been proposed and analysed in the literature [3]-[6]. While the first proposals for converter control strategies explicitly emulating synchronous machine behaviour were developed in the context of distributed generation and microgrids [7],[8], transmission system applications including control of HVDC converter terminals have also been widely studied [9]-[12].

In general, grid forming operation of a VSM-controlled converter requires a dispatchable energy source, in a similar way as any synchronous generator providing primary frequency control in a power system. Thus, a VSC interfaced with an energy storage system or an HVDC converter terminal without responsibility for controlling its dc voltage can be considered the simplest application cases for implementing VSMs [3], [12]. However, inertia emulation by VSM-based control can also be introduced as an ancillary function of power converters in renewable power generation systems such as photovoltaics or wind turbines [2], [3]. In such cases, the primary function of the VSC is to inject a controlled power to the grid according to the Maximum Power Point Tracking (MPPT) for the energy source [13]-[15]. Therefore, the VSM-based control must allow for controlling a time-varying power injection to the grid, while also being able to respond with inertial dynamics to frequency transients in the power system.

In general, VSM-controlled converters in grid connected operation can be easily controlled to follow a slowly varying power reference. However, the grid synchronization mechanism based on a virtual swing equation imposes an inherent trade-off between the emulated inertia, the damping and the speed of response [16]-[18]. Indeed, a VSM with a high virtual inertia will exhibit a relative slow response to variations in the power reference and will require high virtual damping to avoid poorly damped oscillations. Equivalently, a VSM-based control designed for fast transient response to power reference variations cannot provide significant virtual inertia to the power system. Furthermore, the dynamic response will also depend on the equivalent grid impedance [16]. Similar challenges also appear for other control strategies relying on power-balance-based synchronization to the grid voltage, such as the Power Synchronization Control (PSC) [19].

Recently, it has been demonstrated how feed-forward control acting directly on the phase angle of the converter output voltage can be utilized to improve the power reference tracking capability of VSM-controlled converters [20], [21]. However, the implementation in [20] introduced a damping effect that inherently attenuates the inertial response. Furthermore, the phase angle feed-forward in [21] was based on an ideally calculated steady-state power angle. Thus, the effects of non-negligible losses and parameter uncertainties

Manuscript received 20 December 2022; revised 25 February 2023, 17 May 2023, and 27 August 2023; accepted 11 September 2023. Date of publication xx yyy 2023; date of current version: 11 October 2023. This work was supported in part by the project "HVDC Inertia Provision" (HVDC Pro), financed by the ENERGIX program of the Research Council of Norway (RCN) with project number 268053, and the industry partners; Statnett, Equinor, RTE and ELIA, in part by the NorthWind Research Centre for Environment-friendly Energy Research supported by RCN with project number 321954, and in part by the project Ocean Grid Research financed by the RCN with project number 328750. Parts of this manuscript are based on the paper "Improving the Power Reference Tracking of Virtual Synchronous Machines by Feed-Forward Control," presented at the 2020 IEEE 19th International Power Electronics and Motion Control Conference, PEMC 2020, Gliwice, Poland / Virtual Conference, 25-29 April 2021, pp 102-107 [DOI: 10.1109/PEMC48073.2021.9432548]. Approved for publication in the IEEE Transactions on Industry Applications by the Renewable and Sustainable Energy Conversion Systems Committee of the IEEE Industry Applications Society. *(Corresponding author: Jon Are Suul)*

Salvatore D'Arco is with SINTEF Energy Research, Trondheim, Norway,(e-mail: salvatore.darco@sintef.no)

Jon Are Suul is with SINTEF Energy Research, Trondheim, Norway, and also with the Department of Engineering Cybernetics, Norwegian University of Science and Technology, Trondheim, Norway, (e-mail: Jon.A.Suul@sintef.no)

Color versions of one or more figures in this article are available at https://doi.org/...

Digital Object Identifier 10.1109/TIA…

in the calculation of the feed-forward term, combined with the influence of transient dynamics in the electrical system, caused unintended excitation of the VSM inertial dynamics. Another approach for achieving faster power reference tracking of VSM-based control was proposed in [22]. A feed-forward action was introduced from the power reference to the VSM frequency, applying a two-degree of freedom design that allows for specifying the inertial response and the power tracking speed independently. A feed-forward approach for improving the speed of response to power reference variations for PSC has also been proposed in [23]. However, this implementation is based on feed-forward action introduced from the power reference to the current reference of the PSC and is not directly applicable to VSMs.

A feed-forward path from the power reference to the frequency of the VSM swing equation, based on a transfer function with two terms, was also proposed in [24]. However, the purpose of this approach was mainly to damp oscillations, and one of the transfer function terms included a limited derivative action to avoid influencing the steady-state characteristics. Thus, improvement of the power reference tracking was not the main objective. It should also be mentioned that several other recent publications have considered feed-forward control actions for VSM-based control, as for instance [25]-[27]. However, these studies are mainly concerned with the general characteristics and the power decoupling capability of the studied VSM implementations and do not directly consider the power reference tracking capability.

Starting from the concept introduced in [21], this paper presents a Phase Angle Feed-Forward (PAFF) control function that ensures fast and accurate power reference tracking for a VSM. The implementation is based on feed-forward of the steady-state power angle that will result from the power reference, combined with a compensation of the dynamic response in the ac-side power flow based on model inversion. Since low-pass filtering is required for practical implementation of the model inversion, the same filtering effect is also introduced in the power reference. Thus, a fast and accurate but slightly smoothed response to changes in the power reference is achieved. Theoretical derivation of the proposed concept is presented and supported by a frequency domain analysis of a simplified VSM implementation with direct modulation of the output voltage. The results demonstrate how the proposed PAFF control can fully re-shape the power tracking capability of the VSM without influencing the inertial response to grid frequency variations. Application to the Current Controlled VSM (CCVSM) from [28] is presented to verify the performance of the proposed approach for a detailed practical VSM-implementation including a virtual impedance. A parameter sensitivity analysis is also presented to evaluate the impact of the VSM parameters on the dynamic response and the dependency on accurate knowledge of the grid impedance. Finally, the obtained improvement in the power reference tracking of a VSM with the proposed PAFF control is demonstrated by laboratory-scale experimental results.

II. Derivation of Power-Angle Feed-Forward Control for VSMs

The basis for the proposed PAFF control is the general structure of a virtual swing equation combined with the dynamic characteristics of the power flow between two voltage sources, as indicated in Fig. 1. The limitations of the power reference tracking capability of a VSM and the proposed approach for avoiding this limitation by feed-forward control are derived from this starting point.

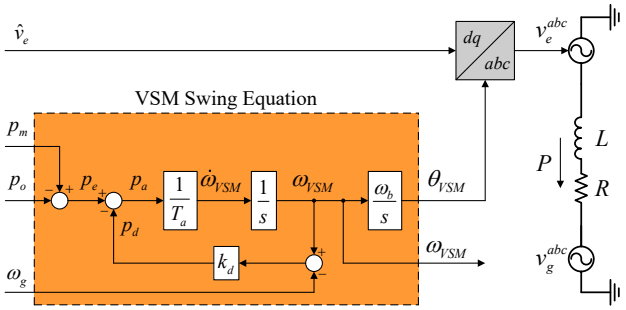

Fig. 1. General illustration of power control by a VSM virtual swing equation generating the voltage phase angle

A. Basic characteristics of VSM

The virtual swing equation of a VSM can be implemented in several different ways. Especially, various approaches have been proposed for emulating the damping effect associated with the damper windings of a synchronous machine [6]. However, for the presented analysis, the details of the implementation are not of significant importance. In the following, the direct implementation of a power balance is preferred since this avoids the need for introducing a nonlinear dependency on the speed [6]. The swing equation in per unit quantities can then be illustrated by Fig. 1 and expressed as:

$$\frac{d\omega_{VSM}}{dt} = \frac{p_m}{T_a} - \frac{p_o}{T_a} - \frac{k_d \cdot (\omega_{VSM} - \omega_g)}{T_a} \tag{1}$$

In this equation ω_{VSM} is the virtual per unit speed of the emulated SM dynamics, p_m represents the emulated mechanical input power to the swing equation and p_o is the electrical output power, while T_a (= $2H$) is the mechanical time constant representing the emulated inertia. The grid frequency is given by ω_g while k_d is the damping coefficient.

As shown in Fig. 1, the phase angle θ_{VSM} associated with the virtual swing equation of a VSM results from integration of the virtual speed, and can be expressed as

$$\frac{d\theta_{VSM}}{dt} = \omega_{VSM} \cdot \omega_b \tag{2}$$

where $\omega_b = 2\pi f_b$ is the base value for the angular frequency, corresponding to the nominal grid frequency. Considering a general network equivalent as indicated on the right-hand side of Fig. 1, the phase angle between the voltage determined by the VSM and the equivalent grid voltage will correspond to the power angle δ_{VSM}, defined as:

$$\frac{d\delta_{VSM}}{dt} = \left(\omega_{VSM} - \omega_g\right) \cdot \omega_b \tag{3}$$

B. Dynamic limitations of VSM-based control schemes

Considering the electrical model with two voltage sources indicated in Fig. 1 and assuming negligible resistance, the steady-state power delivered to the grid can be approximated as [29] :

$$p_o \approx \frac{\hat{v}_e \hat{v}_g}{x} \sin \delta_{VSM} \qquad \frac{\hat{v}_e \hat{v}_g}{x} \quad _{VSM} \tag{4}$$

where $\hat{v}_e$ is the internal voltage amplitude of the VSM while $\hat{v}_g$ is the amplitude of the grid voltage. Furthermore, x is the per unit reactance associated with the inductance L and the grid frequency, while the power angle δ_{VSM} is defined by (3). The value of δ_{VSM} must be small for the approximation of the

sine function to be applicable, but this simplification is only considered as a starting point for preliminary analysis

Assuming a quasi-stationary approximation of the power transfer according to (4), the linearized open loop transfer function from the power deviation p_e (i.e. $p_m - p_o$) indicated in Fig. 1 to the output power p_o can be expressed as [16]:

$$\frac{p_o(s)}{p_e(s)} = \frac{1}{k_d + T_a s} \cdot \frac{\omega_b}{s} \cdot \frac{\hat{v}_e \hat{v}_g}{x} = \omega_b \frac{\hat{v}_e \hat{v}_g}{k_d x} \cdot \frac{1}{1 + \frac{T_a}{k_d} s} \cdot \frac{1}{s} \tag{5}$$

From this equation, it can be seen that the time constant of the open loop transfer function from the power unbalance to the power output will increase for high values of T_a. Furthermore, the dynamic response will have an inherent second order characteristics. These characteristics can be further understood by considering the closed loop transfer function from the power reference p_m to the output power p_o:

$$\frac{p_o(s)}{p_m(s)} = \omega_b \frac{\hat{v}_e \hat{v}_g}{T_a x} \cdot \frac{1}{s^2 + \frac{k_d}{T_a} s + \omega_b \frac{\hat{v}_e \hat{v}_g}{T_a x}} \tag{6}$$

The oscillation frequency, damping and settling time of this closed loop transfer function can be expressed as [16]:

$$\omega_{osc} = \sqrt{\omega_b \frac{\hat{v}_e \hat{v}_g}{T_a x}}, \qquad \xi_{osc} = \frac{1}{2} \sqrt{\frac{x k_d^2}{T_a \omega_b \hat{v}_e \hat{v}_g}},$$
$$T_{set} \approx \frac{4}{\xi_{osc} \omega_{osc}} = \frac{8 T_a}{k_d} \tag{7}$$

These identities clearly show how the oscillation frequency and damping will be reduced while the settling time will increase when the emulated virtual inertia defined by T_a is increased. While an increase of k_d will reduce the settling time, this will also increase the relative damping ξ_{osc} which will attenuate the first swing overshoot that is important for emulating inertial response. Thus, a fast response to power reference variations cannot be directly achieved while providing a strong inertial response to the grid.

As an approach for mitigating the dynamic limitations of the power reference tracking imposed by the virtual inertia of a VSM, a feed-forward control acting directly on the power angle δ_{VSM} was proposed in [21]. This implementation was based directly on calculation of the power angle from the nonlinear expression in (4), resulting in:

$$\delta_{FF} = \sin^{-1}\left(p_m \frac{x}{\hat{v}_e \hat{v}_g} \right), \qquad \theta'_{VSM} = \theta_{VSM} + \delta_{FF} \tag{8}$$

However, due to the dynamic response of the grid impedance, the power flow will not immediately settle to a new steady-state value when imposing direct changes in the phase angle according to changes in the input power p_m in (8). Thus, the dynamic response of the grid impedance will cause the power feedback p_o to transiently deviate from p_m when the power reference to the VSM is changed. This effect will inherently excite the inertial response defined by (6). Thus, even if the approach from [21] could be introduced without influencing the response to grid frequency variations, it could only provide a limited improvement of the power reference tracking capability of the VSM. Indeed, a small excitation of the slow inertial response would always result from changes in the operating conditions, causing inaccurate power reference tracking within the settling time defined by (7). A method for avoiding this issue is proposed in the following, by starting from the derivation of the dynamic response of the power flow to a variation in the VSM phase angle.

C. Mathematical analysis of dynamic relationship between phase angle and power flow

The power flow dynamics in an equivalent grid can be studied by starting from the simplified schematic diagram in Fig. 1. Assuming the phase angle of the grid voltage to be the reference for a space vector-based representation of quantities, the voltage drop in the grid impedance can be modelled in per unit quantities as:

$$\hat{v}_e e^{j\delta_{VSM}} - \hat{v}_g = r \cdot \mathbf{i} + \frac{l}{\omega_b} \frac{d}{dt} \mathbf{i} + j\,\omega_g l \cdot \mathbf{i} \tag{9}$$

where bold symbols represent complex space vectors. The active and reactive power delivered from the equivalent voltage source defined by the VSM can then be expressed as:

$$p_o = \mathrm{Re}\left(\hat{v}_e e^{j\delta_{VSM}} \cdot \breve{\mathbf{i}} \right)$$
$$q_o = \mathrm{Im}\left(\hat{v}_e e^{j\delta_{VSM}} \cdot \breve{\mathbf{i}} \right) \tag{10}$$

As implied by the illustration in Fig. 1, the active and reactive power flows from the VSM are controlled by acting on the voltage amplitude and its phase angle. The dynamic relation between these controllable signals and the power flow is non-linear and not easily obtained in a closed form. However, the derivation of the power flow characteristics can be conveniently split into two parts. Thus, the non-linear steady-state analytical relation between the power and the control variables can be represented as one part, while the dynamic behaviour of the linearized system around an operating point can be represented by the second part.

For steady-state conditions, the voltage balance given by (9) is reduced to:

$$\hat{v}_e e^{j\delta_{VSM}} - \hat{v}_g = r \cdot \mathbf{i} + j\,\omega_g\, l \cdot \mathbf{i}$$

The active and reactive power flow can then be expressed as:

$$p_o = \frac{r\left(\hat{v}_e - \hat{v}_g \cos\delta_{VSM} \right) + \omega_g l \cdot \hat{v}_g \sin\delta_{VSM}}{r^2 + \omega_g^2 l^2} \hat{v}_e$$
$$q_o = -\frac{r \hat{v}_g \sin\delta_{VSM} - \omega_g l \left(\hat{v}_e \hat{v}_g \cos\delta_{VSM} \right)}{r^2 + \omega_g^2 l^2} \hat{v}_e \tag{11}$$

The values of δ_{VSM} and $\hat{v}_e$ corresponding to a specific active and reactive power flow can be solved from these equations. However, the general analytical solution is cumbersome, and a numerical solution will be most practical if accurate results without any further simplifications are required. It can be noted that a very simple solution can be obtained for r=0, which leads to p_o given by (4) and a decoupling of the expressions for p_o and q_o. However, a practical solution to (11) can also be obtained in case of equal and constant voltage amplitudes from both the VSM and the grid (i.e. $\hat{v}_e = \hat{v}_g$). In this case, the VSM phase angle can be obtained from

$$1 - \cos\delta_{VSM} + k_1 \sin\delta_{VSM} = k_2$$
$$k_1 = \frac{\omega_g l}{r} \tag{12}$$
$$k_2 = \frac{2}{3} \frac{r^2 + \omega_g^2 l^2}{r} \frac{p_{ref}}{\hat{v}_g}$$

which gives the solution:

Author Accepted Manuscript version of the paper by Salvatore D'Arco and Jon Are Suul.
in IEEE transactions on industry applications, Vol 60 (2024) Page 851-864, DOI: https://doi.org/10.1109/TIA.2023.3324629

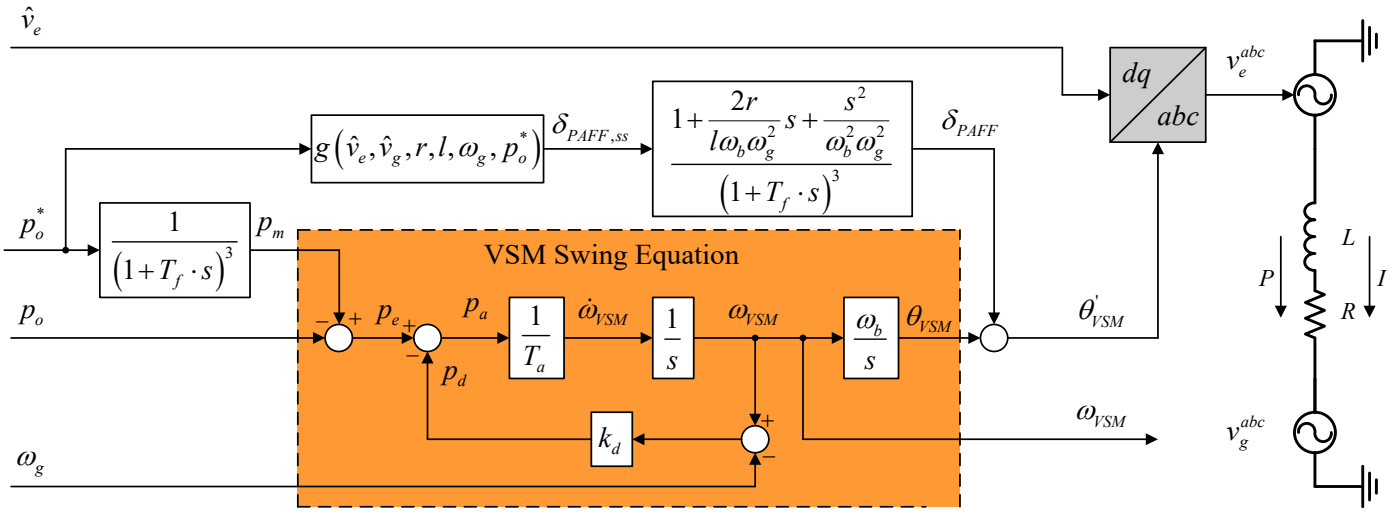

Fig. 2. Proposed implementation of VSM swing equation with dynamic Power Angle Feed-Forward (PAFF) control

$$\delta_{VSM} = \arctan\left(\frac{k_1 - k_1 k_2 \pm \sqrt{k_1^2 + 2k_2 - k_2^2}}{k_2 - 1 \pm k_1\sqrt{k_1^2 + 2k_2 - k_2^2}}\right) \tag{13}$$

The dynamic part of the active and reactive power expressions can be obtained by linearizing the system equations at a steady-state operating point. This leads to the following relationships between the incremental power flow and the voltage amplitude or the phase angle, respectively:

$$\begin{aligned}\frac{\Delta p_o(s)}{\Delta \hat{v}_e(s)} &= \frac{r + \frac{l}{\omega_b}\cdot s}{\underbrace{\omega_g^2 l^2 + \left(r + \frac{l}{\omega_b}\cdot s\right)^2}_{den}}\hat{v}_{e,0} + \frac{p_{o,0}}{\hat{v}_{e,0}} \\ \frac{\Delta p_o(s)}{\Delta \delta_{VSM}(s)} &= \frac{\omega_g l}{\underbrace{\omega_g^2 l^2 + \left(r + \frac{l}{\omega_b}\cdot s\right)^2}_{den}}\hat{v}_{e,0}^2 - q_{o,0}\end{aligned} \tag{14}$$

These expressions imply that a change in the VSM power angle δ_{VSM} will start a transient response in addition to the change of active and reactive power transfer that result from the algebraic equations. The transient response is defined by the poles of the expressions in (14). Since the per unit resistance r is small, the denominator in (14) can be further approximated as.

$$\begin{aligned}den &= r^2 + \omega_g^2 l^2 + 2\frac{l}{\omega_b} r\cdot s + \frac{l^2}{\omega_b^2}\cdot s^2 \\ &\approx \omega_g^2 l^2\left(\frac{1}{\omega_b^2\omega_g^2}s^2 + \frac{2r}{l\,\omega_b\omega_g^2}s + 1\right)\end{aligned} \tag{15}$$

This expression demonstrates that the dynamic response will appear with an undamped resonance frequency equal to the grid frequency and a damping depending on the equivalent resistance or R/X ratio of the grid impedance.

D. Accurate Phase Angle Feed-Forward (PAFF) Control by Model Inversion

The proposed strategy for implementing Phase Angle Feed-Forward (PAFF) control is based on the idea of splitting the steady-state and dynamic parts given by (11) and (14), respectively. Thus, the steady-state power angle $\delta_{PAFF,ss}$ is calculated as a generic nonlinear function of the power reference p_o^*, the voltages, the frequency and the grid impedance, as $g(\hat{v}_e,\hat{v}_g,r,l,\omega_g,p_o^*)$. From this calculation, a step in the power reference will lead to a step in the steady-state power angle corresponding to zero steady-state error. The resulting power angle should then be dynamically processed by a transfer function compensating for the dynamic response of the power flow. For this purpose, a simple model inversion is assumed by introducing zeros defined to cancel the poles from (15). To ensure a strictly proper transfer function that can be easily implemented without significantly influencing the intended model inversion, a third order low-pass filter is introduced. Thus, the general transfer function for defining the final phase angle feed-forward signal is:

$$\delta_{PAFF} = \frac{\frac{1}{\omega_b^2\omega_g^2}s^2 + \frac{2r}{l\,\omega_b\omega_g^2}s + 1}{(1+T_1)(1+T_2)(1+T_3)}\delta_{PAFF,ss} \tag{16}$$

where $\delta_{PAFF,ss}$ is the numerical solution for δ_{VSM} from (11) or the simplified solution from (13). With accurate knowledge of the equivalent resistance and inductance, or the x/r ratio of the grid, the poles associated with the dynamic response in the power flow can be perfectly compensated by the expression in (16). In this case the dynamics will be dictated by the poles of the denominator, defined by the introduced low-pass filter time constants T_1, T_2 and T_3. The selection of these time constants will be discussed in section III and V.

While the pole cancellation introduced in the proposed feed-forward control can ensure a fast and smooth transient of the power flow in response to the feed-forward signal, the VSM swing equation will still respond to deviations between the input power and the measured power flow. Thus, it is proposed to introduce the same low-pass filter as used in the denominator of (16) in the power reference for the VSM. This will imply that the power reference for the VSM swing equation will change with the same dynamic response as the power flow in the circuit imposed by the PAFF control. Thus, the power balance of the VSM swing equation will remain unperturbed, and the inertial response given by (6) will not be excited. The filtering of the input power to the VSM swing equation is then defined by:

$$_m = \frac{1}{(1+T_1)(1+T_2)(1+T_3)}p_o^* \tag{17}$$

An overview of the proposed implementation is shown in Fig. 2, where it is assumed for simplicity that $T_1 = T_2 = T_3 = T_f$. This implementation ensures a significant improvement in the VSM power reference tracking capability, with a

Author Accepted Manuscript version of the paper by Salvatore D'Arco and Jon Are Suul.
in IEEE transactions on industry applications, Vol 60 (2024) Page 851-864, DOI: https://doi.org/10.1109/TIA.2023.3324629

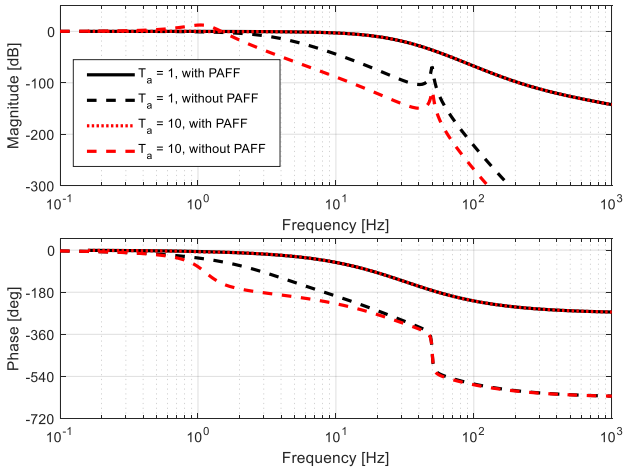

Fig. 3. Frequency response of the transfer function from power reference p_o^* to output power p_o for a generic VSM scheme with and without PAFF

dynamic response defined by the low pass filtering of the power reference, but without influencing the inertial response to grid frequency disturbances. Thus, the VSM with the PAFF control will still provide the same virtual inertia in response to grid frequency variations as without the PAFF.

III. Application to a Generic VSM Scheme

The equivalent transfer functions characterizing the behaviour of a VSM with power feedforward in ideal conditions can be obtained by combining (1), (11) and (16). This assumes a control implementation as shown in Fig. 2 and ideal measurements and modulation. For sake of brevity, the analytical expressions are omitted. The main parameters for the following analysis are defined by k_d = 40 pu, l = 0.5 pu, r = 0.05 pu and $T_1 = T_2 = T_3 = T_f$ =0.005 s. Selecting equal values for all the three time-constants places the corresponding poles at a single controlled location. The value is chosen according to the desired transient response of the power control, as will be discussed in section V.

The Bode plot of the transfer function defined by the power reference as input and active power as output is displayed in Fig. 3. The figure shows the frequency response for two values of T_a when the PAFF function is enabled or disabled. It can be noticed that the introduction of the PAFF control increases the bandwidth with more than a decade and that the resulting frequency characteristics are almost unaffected by T_a. By contrast the cases without the PAFF exhibit a reduced bandwidth for higher values of T_a. This can be easily explained by the considering that any change in the power reference input needs to act on a larger virtual mass and that this virtual mass behaves as a low pass filter.

The behaviour in the frequency domain can be directly confirmed in the time domain by simulations as shown in Fig. 4. The response to a step change in the power reference is shown in Fig. 4 a), where the curves show that the PAFF control ensures a fast overdamped response without any inertial transient. Furthermore, the step response with the PAFF control is unaffected by the value of the inertia time constant. The dynamic response of the scheme without feedforward is in general slower, with longer settling time and an oscillatory inertial behaviour when the value of T_a is high (while k_d, r and l are kept constant). The figure also displays the response when applying a feedforward term containing only the static correction of the phase angle. The corresponding curves highlight how the rapid change in the angle produced by the feedforward excites the oscillatory

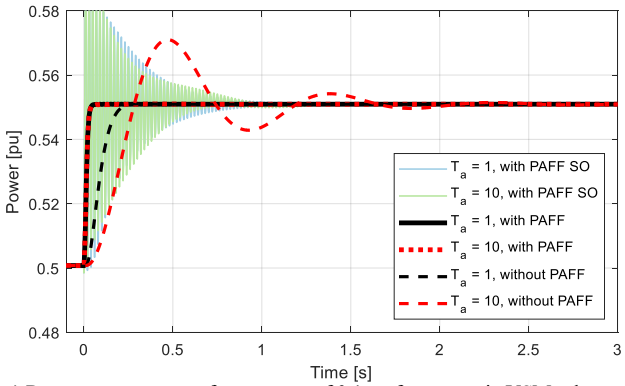

a) Response to power reference step of 0.1 pu for a generic VSM scheme with only the static (SO) PAFF action, with the proposed PAFF implementation and without any PAFF control

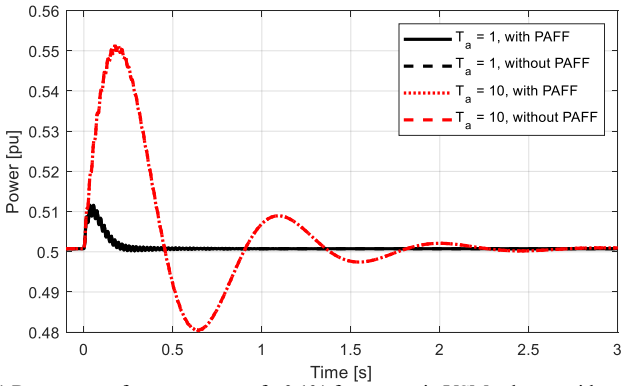

b) Response to frequency step of −0.1% for a generic VSM scheme with and without PAFF control

Fig. 4. Time-domain simulation results illustrating the impact of the proposed PAFF control on the dynamic response of a generic VSM scheme

mode at 50 Hz that can be observed for the cases without PAFF in Fig. 4. These results demonstrate the importance of the dynamic term from (16) in the proposed PAFF control for avoiding poorly damped oscillations.

The results in Fig. 4 b) show the response to a step in the grid frequency and the presented curves illustrate how the inertial response is unaffected by the PAFF control. Indeed, the power responses are identical with and without the PAFF control, and both cases show a more pronounced inertial response with a higher overshoot, lower damping ratio and longer settling time when T_a is high. The results in Fig. 4 a) and b) together illustrate how the PAFF enables operation of a VSM with high virtual inertia while providing fast response to power reference variations.

IV. Application to Detailed VSM Implementation

To demonstrate the applicability and performance of the proposed PAFF control for a relevant practical control scheme, this section presents an analysis of a complete VSM implementation including inner loop current control and a virtual impedance.

A. Studied VSM implementation

The analysis is conducted for a VSM implementation with an inner current control which is relying on a quasi-stationary virtual impedance model for calculating the current references. This control scheme is generally referred to as a current control VSM (CCVSM) as it is directly adapted from [28]. However, the damping in the swing equation is based on grid frequency detection by a PLL as discussed in [30]. An overview of the control scheme is presented in Fig. 5. It should be noted that the calculation of

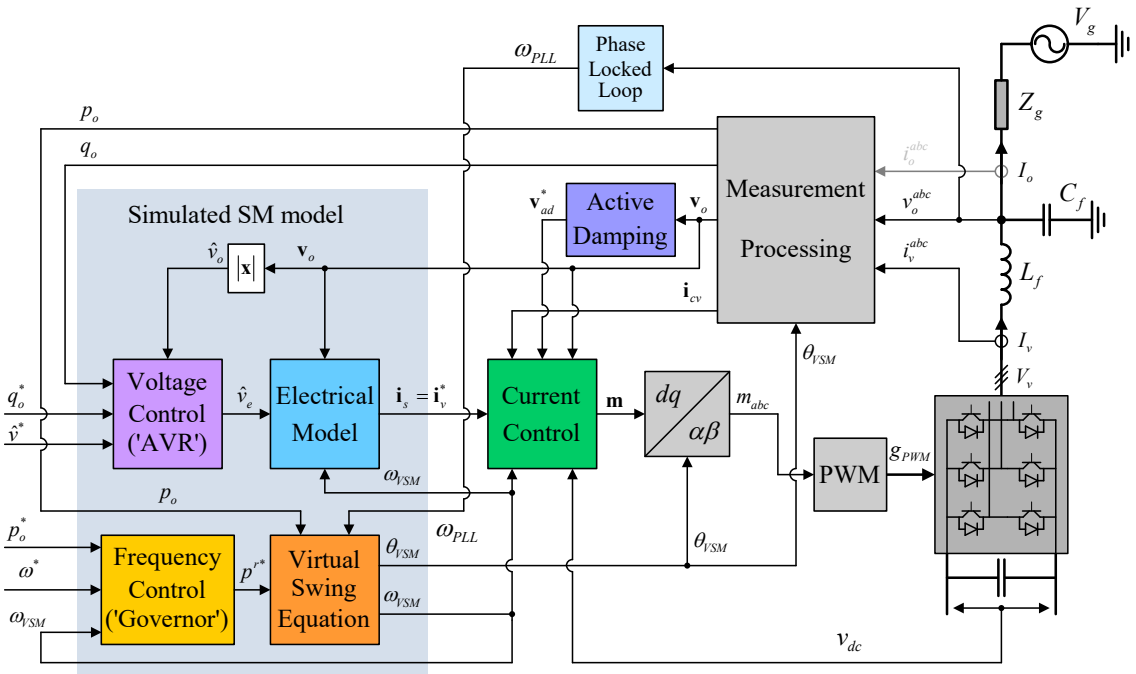

Fig. 5. Control structure of Current Controlled Virtual Synchronous Machine (CCVSM) used for evaluating the performance with Power Angle Feed-Forward (PAFF) control

both the dynamic and steady-state terms in the PAFF control include the virtual impedance of the VSM scheme in addition to the grid impedance. Thus, the generic terms l and r in (11) and (16) are defined as:

$$l = l_s + l_g, \qquad r = r_s + r_g \tag{18}$$

where l_s and r_s represent the virtual impedance while the equivalent grid impedance is given by l_g and r_g. The filter impedance defined by l_f and r_f should not be included in the PAFF control, since it is compensated by the closed loop current control and does not influence the reference frame orientation or power angle of the VSM.

B. *State space modelling and small-signal analysis*

The CCVSM has been modelled according to a state space formulation based on the equations for the individual control functions as presented in [28] and [30]. This results in a model on the general form of

$$\dot{\mathbf{x}} = f(\mathbf{x},\mathbf{u}), \quad \mathbf{y} = g(\mathbf{x},\mathbf{u}) \tag{19}$$

with $\mathbf{x}$ represented by 22 states, whereof 19 states are related to the VSM and 3 states are associated with the low-pass filters applied in the PAFF control. The full non-linear state-space model is reported in the Appendix. This model is then linearized and expressed on standard form [29]:

$$\dot{\mathbf{x}} = \mathbf{A}(\mathbf{x}_0,\mathbf{u}_0)\Delta\mathbf{x} + \mathbf{B}(\mathbf{x}_0,\mathbf{u}_0)\Delta\mathbf{u} \tag{20}$$

An overview of non-zero elements appearing in the A-matrix of the system model are shown in Fig. 6. The matrix can be partitioned into sub-matrices to better highlight the structure of the system. Indeed, the first 19x19 diagonal block includes the terms related to the VSM states only and the other 3x3 diagonal block includes terms associated to the filters of the PAFF control. The two off-diagonal blocks represent the connection between the VSM states and the filter states. The figure clearly shows that only one of these off-diagonal matrix blocks contains non-zero terms. This is because there is an effect of the filter states on the VSM states (i.e. from the last three states on some of the first 19 states) but not vice-versa (i.e. none of the first 19 states influences the 3 last states). Therefore, the system model is represented on a

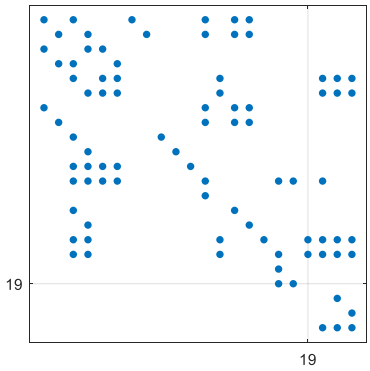

Fig. 6. Overview of non-zero elements in A-matrix of linearized small-signal model representing the studied VSM implementation with added PAFF control

"block-triangular" matrix form [31],[32], For such systems the eigenvalues of the full system can be found by calculating the eigenvalues of the two diagonal blocks independently. Thus, the "block-triangular" property proves that the introduction of the three states associated with the PAFF control does not affect the original eigenvalues of the VSM. Instead, the model is only expanded with three eigenvalues that are not related to the VSM. Thus, the matrix structure in Fig. 6 confirms that the (small-signal) inertial dynamics of the VSM in response to external frequency disturbances, and thereby the inherent feature of providing virtual inertia, are not influenced by the PAFF loop.

C. *Simulation results*

The VSM implementation from Fig. 5 has been simulated in Matlab Simulink, without and with the PAFF control activated, by using the parameters specified in Table I. The same values of T_a and the same perturbations as for the simplified VSM scheme in section III have been used for the simulations. Results for a 0.05 pu step in the power reference are shown in Fig. 7 a). The figure shows how the feedforward term allows the VSM to react faster and with almost negligible overshoot compared to the VSM without the PAFF. However, the transient response of the control loops

Author Accepted Manuscript version of the paper by Salvatore D'Arco and Jon Are Suul.
in IEEE transactions on industry applications, Vol 60 (2024) Page 851-864, DOI: https://doi.org/10.1109/TIA.2023.3324629

TABLE I
PARAMETERS AND SET-POINTS FOR SIMULATIONS

Parameter	Value	Parameter	Value
Rated voltage $V_{S,LL,RMS}$	690 V	Current controller gains: k_{pc}, k_{ic}	1.27 15
Rated power S_b	2.75 MVA	Voltage feed-forward in current controller k_{ffv}	0
Rated ang. freq. ω_b	2π·50 Hz		
Grid voltage $\hat{v}_g$	1.0 pu	Active damping gain k_{ad}	0
Grid angular frequency ω_g	1.0 pu	Active damping filter crossover frequency ω_{ad}	20 rad/s
Grid inductance l_g	0.50 pu	Frequency droop gain k_ω	0
Grid resistance r_g	0.005 pu	PLL PI controller gains, $k_{p,PLL}$, $k_{i,PLL}$	0.0025 0.0013
Filter inductance l_f	0.08 pu		
Filter resistance r_f	0.003 pu	PLL voltage filter, $\omega_{lp,PLL}$	50 rad/s
Filter capacitance c_f	0.074 pu	Reactive power filter ω_{qf}	200 rad/s
Inertia constant T_a	1s or 10 s	Voltage reference $\hat{v}^*$	1.0 pu
Damping coefficient k_d	40	Reactive power reference q^*	0.0 pu
Virtual inductance l_s	0.25 pu	Reactive power droop gain k_q	0.0 pu
Virtual resistance r_s	0.04 pu		
PAFF filter time constants T_1 T_2 T_3	0.005 s	Power reference p^*	0.5 pu
		Frequency ref. ω^*_{VSM}	1.0 pu

that are not considered in the PAFF design, including the current controllers, lead to a transient overshot associated with a small excitation of the inertial dynamics. While this effect did not appear in the ideal case from section III, it has limited practical influence on the studied CCVSM. However, this effect could reduce the performance of the PAFF in case of VSM applications with very low bandwidth of the inner loop current and/or voltage controllers.

The response to a step in the grid frequency is displayed in Fig. 7 b). From the presented curves, it can again be confirmed how the PAFF control does not influence the virtual inertia provided by the VSM.

The time domain simulation model has also been utilized to verify the validity of the linearized small-signal model. While no explicit results are presented for the model verification, the accuracy is as expected, both without and with the PAFF-control activated, in line with the results presented for the CCVSM in [28].

D. Frequency domain analyis

The improvement in the power tracking performance achieved with the PAFF control can also be evaluated in the frequency domain. For this purpose, the transfer function from the power reference to the power output is extracted from the detailed small-signal state-space model. The resulting Bode diagram is shown in Fig. 8, and the plotted curves show how the PAFF control increases the bandwidth of the transfer function with more than one decade. At lower frequencies (i.e. < 30 Hz), the frequency response with the PAFF is almost identical to the response when applying the PAFF to the ideal VSM scheme evaluated in Fig. 3. However, visible differences can be noticed at higher frequency with a significant notch at 50 Hz and a smaller notch at around 400 Hz. These variations can be attributed to the inner loops that are included in the detailed scheme and not present in the generic scheme from Fig. 2. Still, the figure shows how the power control bandwidth with the PAFF control is almost independent from the emulated inertia. It can also be noted that the frequency characteristics for the cases without the PAFF control in Fig. 8 are different from the ideal cases with the simplified VSM in Fig. 3. For instance, the plots without PAFF control in Fig. 3 exhibit a clear resonance at 50 Hz, which is not visible in Fig. 8 since it is mitigated by the closed loop current control.

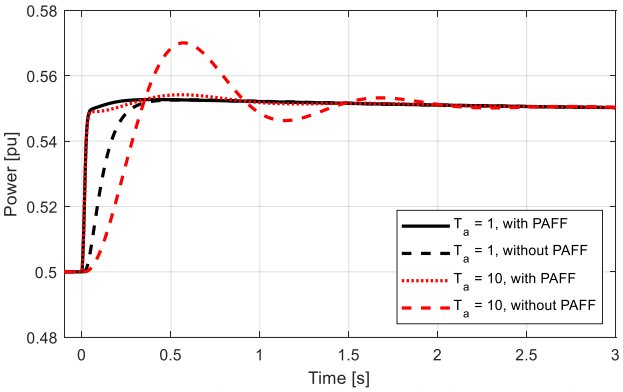

a) Response to power reference step of 0.05 pu for the CCVSM scheme with and without PAFF control

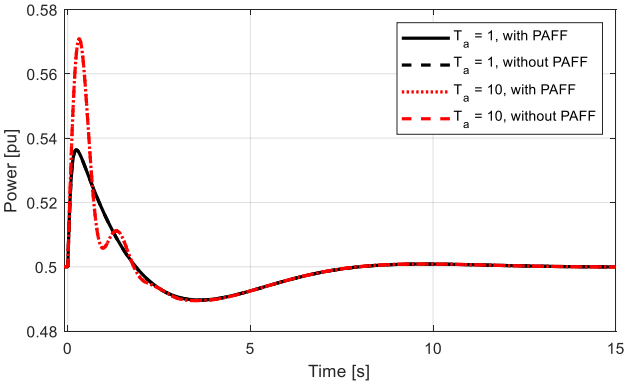

b) Response to frequency step −0.1% for the CCVSM scheme with and without PAFF control

Fig. 7. Time-domain simulation results illustrating the impact of the proposed PAFF control on the dynamic response of a CCVSM

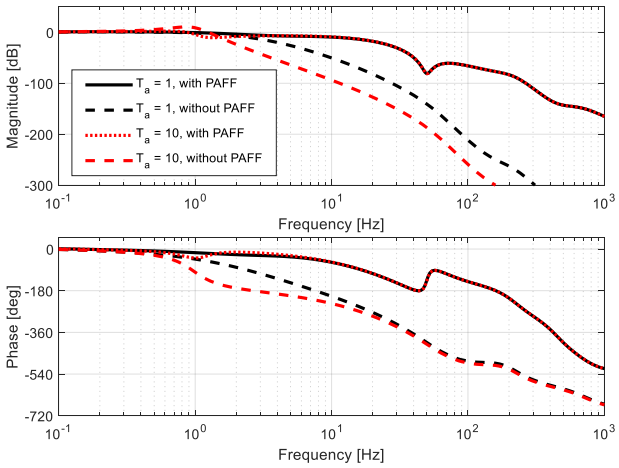

Fig. 8. Bode plot for the transfer function from power reference to output power for a CCVSM scheme VMS with and without PAFF

V. IMPACT FROM PARAMETRIC VARIATIONS

While the PAFF control adds a feedforward term by assuming knowledge of the grid impedance, the grid impedance can exhibit large variations and may not be accurately known. Thus, it is relevant to assess the performance of the PAFF for a wide range of grid conditions and its robustness against errors in the assumed grid impedance.

A. Grid impedance variations

For assessing the performance with PAFF control in different grid conditions, four values of the equivalent grid inductance are considered (i.e. 0.05 pu, 0.1 pu, 0.2 pu, and 0.5 pu), while the equivalent grid resistance is kept constant

Author Accepted Manuscript version of the paper by Salvatore D'Arco and Jon Are Suul.
in IEEE transactions on industry applications, Vol 60 (2024) Page 851-864, DOI: https://doi.org/10.1109/TIA.2023.3324629

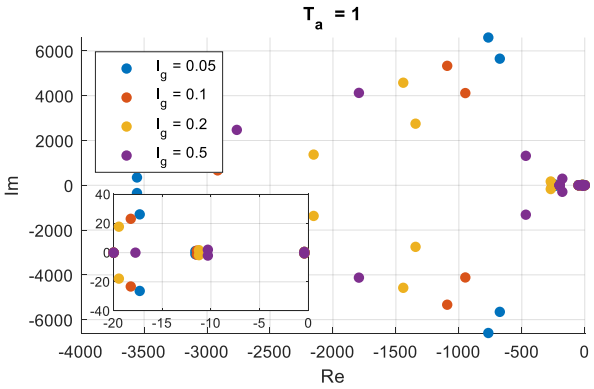

a) Eigenvalues of the studied system for different values of the grid inductance l_g between 0.05 pu (SCR = 20)- and 0.5 pu (SCR = 2) for T_a = 1 s

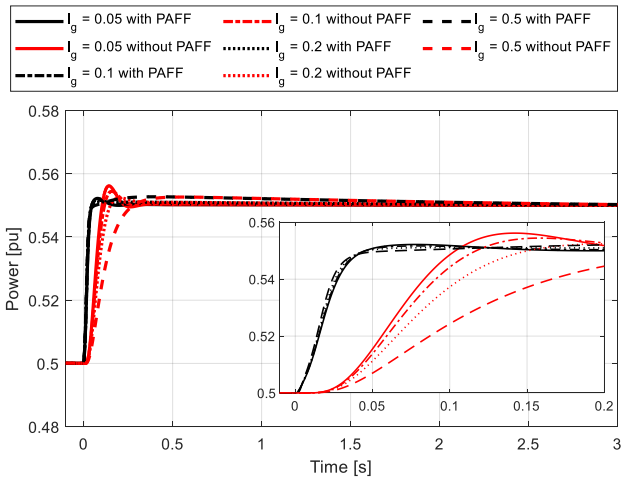

b) Time response with different grid impedance values without and wtith the PAFF control for T_a = 1 s

Fig. 9. Eigenvalues and time-response with T_a = 1 s and different values of grid impedance

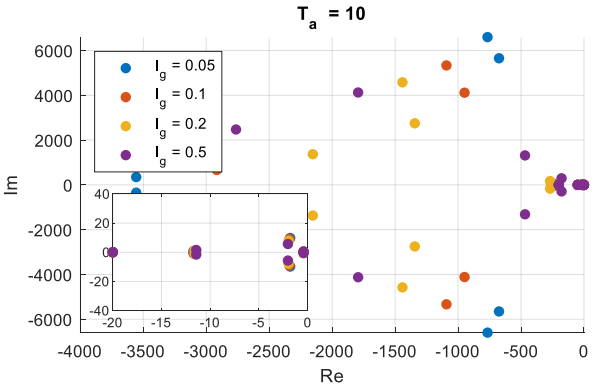

a) Eigenvalues for different values of the grid inductance l_g between 0.05 pu (SCR = 20) and 0.5 pu (SCR = 2) for T_a = 10 s

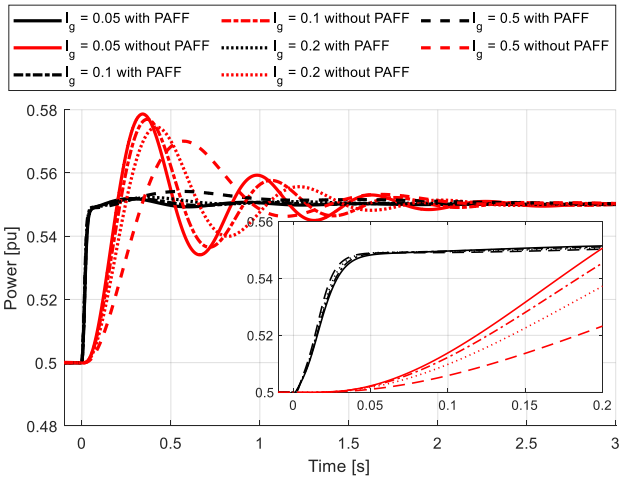

Time response with different grid impedance values without and wtith the PAFF control for T_a = 10 s

Fig. 10. Eigenvalues and time-response with T_a = 10 s and different values of grid impedance

at 0.05 pu. It is still assumed that the values of the resistance and the inductance are known for the PAFF operation. It should also be noted that the control scheme includes the additional virtual impedance as given in Table I.

Fig. 9 a) shows the eigenvalues of the studied system for the different values of the grid inductance when T_a = 1s. The figure clearly shows how the oscillation frequency and settling time of the high frequency modes are decreasing when the grid inductance is increasing. Furthermore, the zoomed plot in the figure shows how the mode associated with the inertial response is becoming more damped and finally bifurcates into two real eigenvalues when the grid impedance is increased. Since the PAFF control does not affect the eigenvalues of the system, the results in Fig. 9 a) are identical both without and with the PAFF path activated. However, the influence from the PAFF control on the time response is clearly seen in Fig. 9 b). This figure shows how the response in the power flow without the PAFF control is becoming more damped when the inductance is increased, as expected from the eigenvalue analysis. However, with the PAFF control activated, the time response is almost independent from the grid impedance, as shown by the black curves. Instead, the time response is mainly determined by the low pass filtering introduced in the model inversion and power reference signal.

The differences between the control without and with the proposed PAFF control are even more clear when the inertia time constant is increased to Ta = 10 s. The eigenvalues for different grid impedances values are shown in Fig. 10 a), and the main difference from the case of Ta = 1 s is that the eigenvalues associated with the inertial dynamics have higher real part and thereby a less damped response with a longer settling time. The consequence is clearly seen for the case without the PAFF control by the red curves in Fig. 10 b). These results clearly demonstrate the limitation in the power reference tracking of the regular VSM control with a high inertia, which causes high overshoot and long settling time. For the cases with the PAFF control activated, the initial time response is almost independent from the grid impedance. However, a small excitation of the inertial dynamics can be seen from the black curves in Fig. 10 b), due to the non-ideal response of the control system to the phase shift imposed by the PAFF control. As the impact from the transient response is small, it can still be concluded that the PAFF control can provide a relatively fast and consistent response to power reference variations for any value of the grid impedance.

B. Impact of low pass filter time constant

As mentioned in section III, it is preferred to keep the same value for all the three low pass filter time constants utilized for the model inversion and power reference filtering. The value of this common filter time constant, T_f, can then be selected to shape the response to the power reference variations. A set of plots showing the impact of T_f on the response to a step in the power reference is shown in Fig. 11. From the zoomed plot in the figure, it can be seen

Author Accepted Manuscript version of the paper by Salvatore D'Arco and Jon Are Suul.
in IEEE transactions on industry applications, Vol 60 (2024) Page 851-864, DOI: https://doi.org/10.1109/TIA.2023.3324629

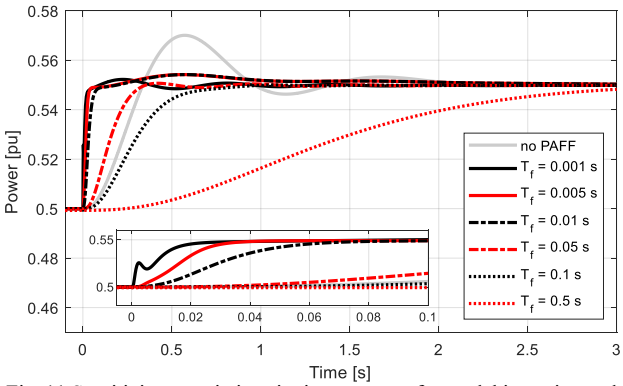

Fig. 11.Sensitivity to variations in time constant for model inversion and low-pass filtering of power reference

that a very low value of T_f can cause excitation of some relatively fast transients. However, high values of T_f can make the rise time of the power flow even longer than for the original VSM without the PAFF control. As a smooth power response with a rise-time shorter than without the PAFF control is preferred, the value of T_f should generally be chosen in the range between 5 ms and 50 ms. As a fast response is prioritized in this paper, the value of 5 ms is used for all other cases than the plots shown in Fig. 11.

C. *Sensitivity to parameter deviations*

Since the PAFF control is based on a feedforward compensation of the phase angle for the VSM reference frame orientation, its performance is linked to the knowledge of the total equivalent impedance. Thus, any error in the applied values for inductance or resistance will cause a nonideal response that will excite the inertial dynamics of the VSM. As already mentioned, the equivalent impedance considered by the PAFF includes both the physical impedance of the external circuit, which in principle is unknown, and the virtual impedance, which is a tuning parameter for the VSM. Thus, it is important to note that the presence of the virtual impedance effectively reduces the sensitivity of the PAFF performance to errors in the external impedance. Especially when the virtual impedance is high, a large relative deviation in the grid impedance can still correspond to a limited relative error in the total impedance.

The effect of a deviation between the actual and assumed equivalent grid impedance on the power reference tracking is shown in Fig. 12 for the two cases of T_a = 1 s and T_a = 10 s. In these plots, an error varying between 1% and 30% has been intentionally introduced in the value for the equivalent grid impedance (i.e. with constant *l*/*r* ratio) when calculating the terms of the PAFF control. The results indicate that the feedforward correction still ensures a short rise time of the power flow, but the value reached after the fast initial increase of power flow is deviating more from the reference value with higher values of the error. The deviation is then compensated by the VSM power control mechanism, but this results in the excitation of an inertial transient with an amplitude that increases with higher values of the error.

In general, the presented results indicate that the PAFF is relatively robust with respect to errors in the assumed grid impedance. While parameter deviations will deteriorate the performance and cause a small excitation of the inertial dynamics, a much faster response with a significantly reduced overshoot is still achieved compared to the case without the PAFF, even with a 30% error in the equivalent impedance. Thus, the transient response to power reference variations with the PAFF control is still preferrable

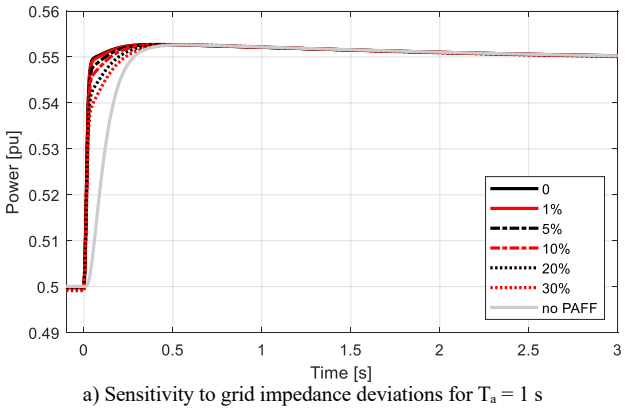

a) Sensitivity to grid impedance deviations for T_a = 1 s

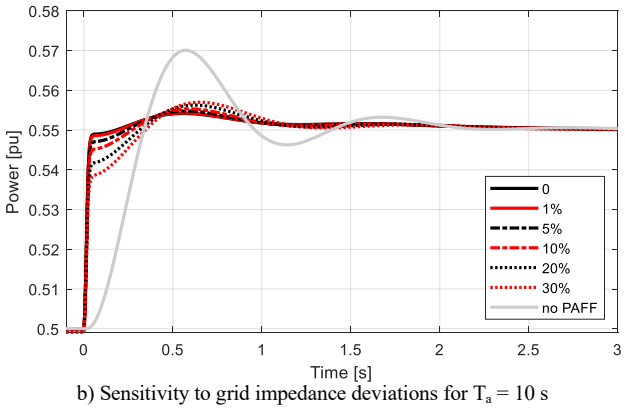

b) Sensitivity to grid impedance deviations for T_a = 10 s

Fig. 12. Sensitivity of the response to power reference variation with errors in the grid impedance

compared to the case without any feed-forward compensation, especially when the emulated inertia is high.

VI. Experimental Validation

The performance and applicability of the proposed PAFF control for the CCVSM from Fig. 5 has been validated experimentally with a 50 kV, 400V prototype of a 2 level VSC. The converter is connected to a 200 kVA grid emulator that allows to impose controlled grid conditions including step variations of the frequency. Both the converter and the grid emulator are controlled by an OPAL-RT OP5600 platform for real time simulation and rapid prototyping. However, the pulse width modulation (PWM) and the inner loop current controllers are implemented on the field programmable gate array (FPGA) of a Zynq 7030 System on Chip (SoC), which is included in a local control board that also provides signal conditioning and A/D conversion of the measurements being transmitted to the OPAL-RT platform. The Zynq-based control board and the corresponding fibre-optic communication links are further described in [33]. For the conducted experiments, the control loops implemented in the OPAL-RT are operated with a sampling frequency of 10 kHz, while the inner loop current controllers implemented on the FPGA are operated with a sampling frequency of 40 MHz. A schematic overview of the experimental setup is shown in Fig. 13, and a set of photos from the laboratory environment with indications of the main elements are shown in Fig. 14. The main parameters of the system are listed in Table II. A video showing the main elements of the experimental setup and the process of obtaining results is also included as a multimedia attachment to the paper.

A first test has been conducted by applying a step in the power reference with the PAFF function enabled or disabled. The results for four values of T_a (i.e., T_a =1 s, 2s, 5s, and 10

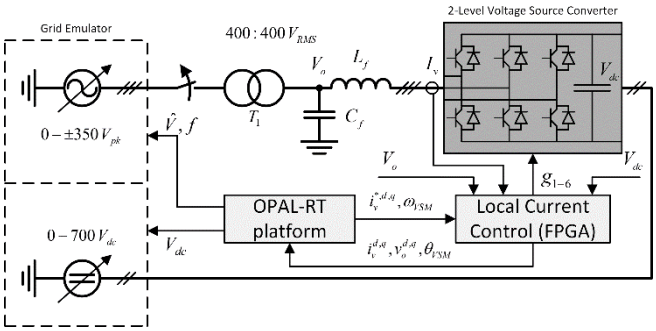

Fig. 13. Overview of circuit configuration for experimental setup

Fig. 14. Photos of experimental setup

TABLE II
PARAMETERS AND SET-POINTS FOR EXPERIMENTAL TESTS

Parameter	Value	Parameter	Value
Rated voltage $V_{S,LL,RMS}$	400 V	Inertia constant T_a	1,2,5,10 s
Rated power S_b	50 kVA	Damping coefficient k_d	40
Rated ang. freq. ω_b	2π·50 Hz	SM inductance l_s	0.25 pu
Grid voltage $\hat{v}_g$	1.0pu	SM resistance r_s	0.01 pu
Grid angular frequency ω_g	1.0 pu	Frequency droop gain k_ω	0
Grid inductance l_g	0.21 pu	Voltage reference $\hat{v}^*$	1.0 pu
Grid resistance r_g	0.025 pu	Reactive power ref. q^*	0.0 pu
Filter inductance l_f	0.05 pu	Reactive power droop gain k_q	0.0 pu
Filter resistance r_{lf}	0.01 pu	Power reference p^*	0.0 pu
Filter capacitance c_f	0.050 pu	Frequency ref. ω^*_{VSM}	1.0 pu

s) are presented in Fig. 15. The plotted curves show how the feedforward control enables a fast response with negligible oscillations in the active power. Moreover, the behaviour is practically independent from the value of T_a while the regular VSM scheme without the PAFF control shows an oscillatory inertial response when T_a is increased. The difference in dynamic response is also indicated by Fig. 16 which shows the sampled values of the instantaneous phase voltages measured at the filter capacitance (in grey) and the converter output currents. The plots are presented for the case of T_a = 1 s without and with the PAFF control. The presented curves are clearly illustrating how the currents for the case with PAFF control are quickly and smoothly settling to a new steady-state operating condition without the inertial response seen in the case without the feed-forward (FFW) path activated.

Results from the experimental tests also confirm that the schemes with the PAFF control enabled and disabled behave identically when exposed to a perturbation in the grid frequency. One example for the case of T_a = 2s is presented in Fig. 17, which shows the response in the active power for a step of −0.05 Hz (−0.1 %) in the grid frequency. The negligible differences between the two curves shown in the figure are only related to differences in noise during two

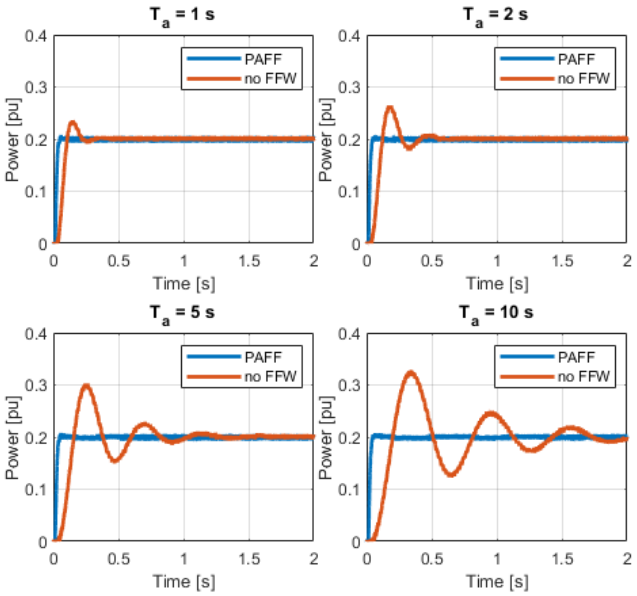

Fig. 15. Experimental results showing the response to variations in the power reference with different values of T_a

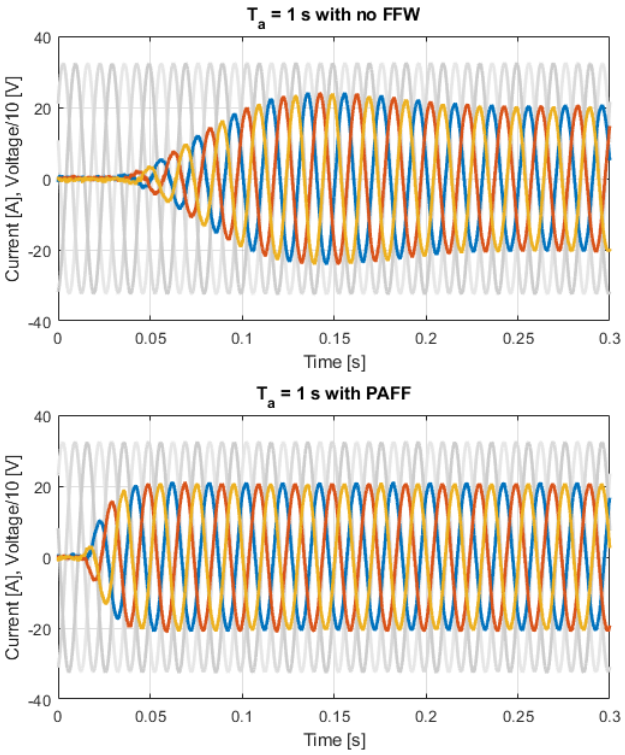

Fig. 16. Instantaneous voltage and current waveforms without and with the PAFF control for the case with T_a = 1 s

consecutive experimental tests, while it is clearly seen that the inertial response is identical for the two cases.

Finally, the sensitivity of the PAFF control to deviations in the equivalent impedance has been verified by experiments. For simplicity, the value of the virtual impedance has been set differently from the value used in the calculations for the PAFF, even though the value of the virtual impedance is known exactly in practice. This allowed for simpler testing than by changing the impedance in the electrical circuit by adding a physical impedance in series to the output transformer. The effect of variations in the total inductance is shown in Fig. 18. The results confirm how the PAFF function is sensitive to errors in the grid impedance since both the steady state angle calculation and the dynamic

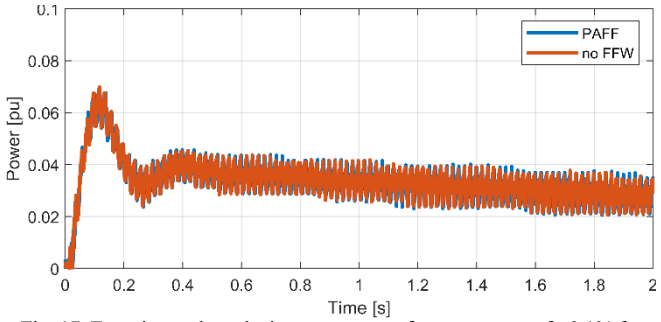

Fig. 17. Experimental results in response to a frequency step of −0.1% for the CCVSM scheme with and without the proposed PAFF control

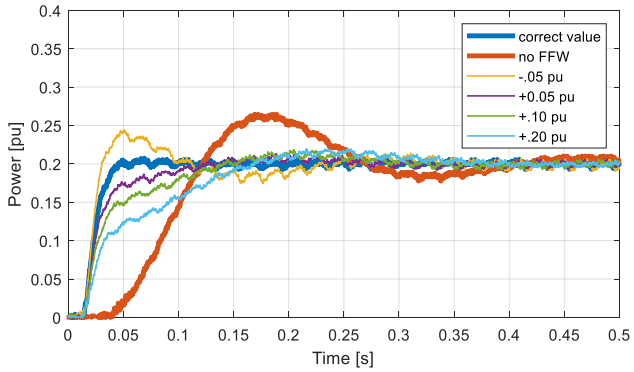

Fig. 18. Response to power reference step of 0.2 pu with $T_a = 2$ s and different deviations from the value of the total equivalent inductance used in the calculation of the PAFF terms

compensation of the filter resonance are affected. The performance of the control clearly deteriorates with increasing deviation in the inductance. As discussed for the simulation results, the main reason is that the change of phase angle provided by the PAFF does not directly result in the required change of power flow when the impedance values do not coincide with the actual sum of the grid impedance and the virtual impedance. As shown by the figure, a lower inductance than assumed for the PAFF control causes an initial power transient that exceeds the reference. Similarly, a higher impedance than assumed for the PAFF control causes an initial power flow that is too low. In both cases, the remaining part of the transient is dictated by the behaviour of the virtual swing equation, which implies that the transient will become longer and more oscillatory for high values of T_a. However, even if the performance is partly worsened by parameter deviations, the overall performance with the PAFF control is still better than when it is disabled. This indicates that it is critical to provide an accurate estimation of the grid impedance but also that the scheme shows a form of robustness and tolerance to variations in the grid impedance. Moreover, it should be considered that these effects will be even smaller in relative terms when applying a larger virtual impedance, because the relative uncertainty in the total equivalent impedance value will be smaller.

VII. Conclusion

This paper has presented an approach for improving the power reference tracking performance of VSM-based control schemes relying on a simulated swing equation. The improved response is obtained by adding a power angle feed-forward (PAFF) term directly to the phase angle resulting from the swing equation utilized for inertia emulation and power-balance-based grid synchronization. This feedforward term does not affect the modes of the system and the response to grid disturbances. Thus, the PAFF does not alter the stability characteristics, the power synchronization mechanism or the grid forming capabilities of the VSM. The increased bandwidth for reference tracking and the higher responsiveness can be necessary to provide virtual inertia by the VSM while retaining a similar controllability of the power injected to the grid as for converters with "grid-following" control. This will be especially important if it is desirable to provide a high virtual inertia.

The performance of the PAFF control in increasing the power reference tracking capabilities without affecting the response to grid frequency disturbances is proven by time-domain simulation, frequency domain analysis and experimental verification. The presented results confirm that rise time and tracking bandwidth are increased as intended. Examples of potential applications for the proposed PAFF control in VSMs that could be further investigated include wind turbines, photovoltaic generators, HVDC terminals and energy storage systems intended to provide multiple ancillary services to the grid.

References

[1] B. Muftau, M. Fazeli, "The Role of Virtual Synchronous Machines in Future Power Systems: A Review and Future Trends," in *Electric Power System Research*, Vol 206, Article Number 10775, 17 pp., May 2022

[2] J. Fang, H. Li, Y. Tang, and F. Blaabjerg, "On the inertia of future more electronics power systems," in *IEEE Journal of Emerging and Selected Topics in Power Electronics*, Vol. 7, No. 4, pp. 2130–2146, December 2019

[3] K. M. Cheema, "A comprehensive review of virtual synchronous generator," in *Electric Power System Research*, Vol. 120, Article Number 106006, 10 pp., September 2020

[4] H. Alrajhi Alsiraji, R. El-Shatshat, "Comprehensive assessment of virtual synchronous machine based voltage source converter controllers," in *IET Generation, Transmission, Distribution*, Vol. 11, No. 7, pp. 1762–1769, May 2017

[5] V. Mallemaci, F. Mandrile, S. Rubino, A. Mazza, E. Carpaneto, R. Bojoi, "A comprehensive comparison of Virtual Synchronous Generators with focus on virtual inertia and frequency regulation," in *Electric Power System Research*, Vol. 201, Article Number 107516, 13 pp., December 2021

[6] S. D'Arco, J. A. Suul, "Virtual Synchronous Machines – Classification of Implementations and Analysis of Equivalence to Droop Controllers for Microgrids," in *Proc. of the IEEE PowerTech Grenoble 2013*, Grenoble, France, 16-20 June 2013, 7 pp.

[7] H.-P. Beck, R. Hesse, "Virtual Synchronous Machine," in *Proceedings of the 9th International Conference on Electrical Power Quality and Utilisation*, Barcelona, Spain, 9-11 October 2007, 6 pp.

[8] K. Sakimoto, Y. Miura, T. Ise, "Stabilization of a power system with a distributed generator by a virtual synchronous generator function," in *Proceedings of the 8th International Conference on Power Electronics – ECCE Asia*, Jeju, Korea, 30 May- 3 June 2011, 8 pp.

[9] M. Guan, W. Pan, J. Zhang, Q. Hao, J. Cheng, X. Zheng, "Synchronous Generator Emulation Control Strategy for Voltage Source Converter (VSC) Stations," in *IEEE Transactions on Power Systems*, Vol. 30, No. 6, pp. 3093-3101, November 2015

[10] R. Aouini, B. Marinescu, K. B. Kilani, M. Elleuch, "Synchronverter-Based Emulation and Control of HVDC Transmission," in *IEEE Trans. on Power Systems*, Vol. 31, No. 1, pp. 278-286, January 2016

[11] W. Zhang, K. Rouzbehi, A. Luna, G. B. Gharehpetian, P. Rodriguez, "Multi-terminal HVDC grids with inertia mimicry capability," in *IET Renewable Power Generation*, Vol. 10, No. 6, pp. 752-760, July 2016

[12] S. D'Arco, G. Guidi, J. A. Suul, "Operation of a Modular Multilevel Converter Controlled as a Virtual Synchronous Machine," in *Proceedings of the International Power Electronics Conference*, IPEC 2018 ECCE Asia, Niigata, Japan, 20-24 May 2018, 8 pp.

[13] Q.-C. Zhong, "Virtual Synchronous Machines: A unified interface for grid integration," in *IEEE Power Electronics Magazine*, Vol. 3, No. 4, pp. 18-27, December 2016

[14] A. Tarraso, J. I. Candela, J. Rocabert, P. Rodriguez, "Synchronous Power Control for PV Solar Inverters With Power Reserve

Capability," in *Proceedings of the 43rd Annual Conference of the IEEE Industrial Electronics Society*, IECON 2017, Beijing, China, 29 October – 1 November 2017, pp. 2712-2717

[15] B. A. Bastiani, R. Vasques de Oliveira, "Adaptive MPPT control applied to virtual synchronous generator to extend the inertial response of type-4 wind turbine generators," in *Sustainable Energy, Grids and Networks*, Vol. 27, Article Number 100504, 13 pp., September 2021

[16] F. Wang, L. Zhang, X. Feng, H. Guo, "An Adaptive Control Strategy for Virtual Synchronous Generator," in *IEEE Transactions on Industry Applications*, Vol. 54, No. 5, pp. 5124-5133, September 2018

[17] Z. Wang, F. Zhou, J. Wu, H. Zhai, Z. Zeng, "Inertia time constant design in microgrids with multiple paralleled virtual synchronous generators," in *Proceedings of the 2017 19th European Conference on Power Electronics and Applications*, EPE'17 ECCE Europe, Warsaw, Poland, 11-14 September 2017, 9 pp-

[18] Z. Wang, F. Zhou, H. Yi, J, Wu, F. Wang, Z. Zeng, "Analysis of Dynamic Frequency Performance Among Voltage-Controlled Inverters Considering Virtual Inertia Interaction in Microgrid," in *IEEE Transactions on Industry Applications*, Vol. 55, No. 4, pp. 4135-4144, July/August 2019

[19] L. Zhang, L. Harnefors, H.-P. Nee, "Power Synchronization Control of Grid-Connected Voltage-Source Converters," in *IEEE Transactions on Power Systems*, Vol. 25, No. 2, pp. 809-820, May 2010

[20] M. Li, Y. Wang, H. Zhou, W. Hu, "A Phase Feedforward Based Virtual Synchronous Generator Control Scheme," in *Proceedings of the 2018 IEEE Applied Power Electronics Conference*, APEC 2018, San Antonio, Texas, USA, 4-8 March 2018, pp. 3314-3318

[21] S. D'Arco, J. A. Suul, "Improving the Power Reference Tracking of Virtual Synchronous Machines by Feed-Forward Control," in *Proceedings of the 2021 IEEE 19th International Power Electronics and Motion Control Conference*, PEMC 2020, Gliwice, Poland / Virtual Conference, 25-29 April 2021, pp 102-107

[22] A. E. Leon and J. M. Mauricio, "Virtual Synchronous Generator for VSC-HVDC Stations With DC Voltage Control," in *IEEE Transactions on Power Systems*, vol. 38, no. 1, January 2023, pp. 728-738

[23] L. Harnefors, F. M. M. Rahman, M. Routimo, "Reference-Feedforward Power-Synchronization Control," in *IEEE Trans. on Power Electronics*, Vol. 35, No. 9, September 2020, pp. 8878-8881

[24] Y. Yu, S. K. Chaudhary, G. D. A. Tinajero, L. Xu, N. N. B Abu Bakar, J. C. Vasquez, J. M. Guerrero, "A Reference-Feedforward-Based Damping Method for Virtual Synchronous Generator Control," in *IEEE Transactions on Power Electronics*, Vol. 37, No. 7, July 2022, pp. 7566-7571

[25] T. Wen, X. Zou, X. Guo, D. Zhu, L. Peng and X. Wang, "Feedforward Compensation Control for Virtual Synchronous Generator to Improve Power Decoupling Capability," in *Proceedings of the 14th IEEE Conference on Industrial Electronics and Applications*, ICIEA 2019, Xian, China, 19-21 June 2021, 6 pp.

[26] M. G. Ippolito, R. Musca, G. Zizzo, "Fundamental Analysis of Grid-Forming Converters Enhanced with Feedforward Controls," in *Proceedings of the 2022 International Conference on Power Energy Systems and Applications*, ICoPESA 2022, Singapore, 25-27 February 2022, pp. 312-318

[27] A. Liu, J. Liu, Q. Wu, "Improvement of VSG Transient Performance Based on Power Feedforward Decoupling Control," in *IET Generation, Transmission and Distribution*, Vol. 16, NO. 20, October 2022, pp. 4080–4095

[28] O. Mo, S. D'Arco, J. A. Suul, "Evaluation of Virtual Synchronous Machines with Dynamic or Quasi-stationary Machine Models," in *IEEE Trans. Ind. Electron.*, Vol. 64, No. 7, pp. 5952-5962, July 2017

[29] P. Kundur, "*Power System Stability and Control*," New York: McGraw-Hill Education, 1994

[30] S. D'Arco, J. A. Suul, O. B. Fosso, "A Virtual Synchronous Machine Implementation for Distributed Control of Power Converters in SmartGrids," in *Electric Power System Research*, Vol. 122, pp. 180-197, May 2015

[31] J. R. Silvester, "Determinants of Block Matrices," in The *Mathematical Gazette*, vol. 80, no. 501, pp. 460-467, Nov. 2000

[32] G. Bergna, S. D'Arco, J. A. Suul, "Impact on Small-Signal Dynamics of Using Circulating Currents Instead of AC-Currents to Control the DC Voltage in MMC HVDC Terminals," in *Proceedings of the 2016 IEEE Energy Conversion Congress and Exposition*, ECCE 2016, Milwaukee, Wisconsin, USA, 18-22 September 2016, 8 pp.

[33] K. Ljøkelsøy, G. Guidi, "Development of a scale model of a Modular Multilevel Converters," in *Proc. 14th Deep Sea Offshore Wind R&D Conference*, EERA DeepWind'2017, 18-20 January 2017, Trondheim Norway, *Energy Procedia*, Vol. 137, October 2017, pp. 505-513

APPENDIX

The complete state-space model of the studied CCVSM implementation from Fig. 5 is defined by the 22 equations given below, where the expression for k_3 is given by:

$$k_3 = \delta_0 + \frac{k_\delta}{T_1 T_2 T_3}\left(z_1 + \frac{2}{\omega_b^2 \omega_g^2}\frac{r_{est}}{l_{est}} z_2 + \frac{1}{\omega_b^2 \omega_g^2} z_3 \right)$$

The variables not previously defined in the text are adapted from [28] and [30] and include:

- γ integral state of current error in PI current controllers
- ϕ low pass filtered voltage for active damping
- v_n grid voltage
- $\delta\theta_{VSM}$ phase angle difference between grid voltage and virtual rotor voltage
- $k_{ff\delta}$ coefficient to enable PAFF control
- v_{om} low pass filtered output voltage
- ε_{PLL} integral error for PI controller of PLL
- ω_n grid angular frequency
- δ_0, k_δ coefficients from linearization of P(δ) function
- r_{est} estimated grid resistance for PAFF control
- l_{est} estimated grid inductance for PAFF control

$$1)\ s\cdot i_{l,d} = -\frac{k_{pc}+r_f}{l_f}\omega_b i_{l,d} + \omega_b\,\omega_g\,i_{l,q} - \frac{1+k_{ad}-k_{ffv}}{l_f}\omega_b v_{o,d} + \frac{k_{ic}\,\omega_b}{l_f}\gamma_d + \frac{k_{ad}\,\omega_b}{l_f}\phi_d - \omega_b\,i_{l,q}\,\omega_{VSM}$$
$$- \frac{k_q\,r_s\left(q_m - q^*\right) + r_s\,v_{om,d} - r_s\,\hat{v}^* + l_s\,v_{om,q}\,\omega_{VSM}}{l_f\left(r_s^2 + \omega_{VSM}^2 l_s^2\right)} k_{pc}\,\omega_b$$

$$2)\ s\cdot i_{l,q} = -\frac{k_{pc}+r_f}{l_f}\omega_b i_{l,q} - \omega_b\omega_g i_{l,d} - \frac{1+k_{ad}-k_{ffv}}{l_f}\omega_b v_{o,q} + \frac{k_{ic}\,\omega_b}{l_f}\gamma_q + \frac{k_{ad}\omega_b}{l_f}\phi_q + \omega_b\,i_{l,d}\,\omega_{VSM}$$
$$+ \frac{k_q\,r_s\left(q_m - q^*\right) + r_s v_{om,d} - r_s\hat{v}^* + l_s v_{om,q}\omega_{VSM}}{l_f\,r_s\left(r_s^2 + \omega_{VSM}^2 l_s^2\right)} k_{pc} l_s \omega_b \omega_{VSM} \quad \frac{k_{pc}\,v_{om,q}\,\omega_b}{l_f r_s}$$

3) $s \cdot v_{o,d} = -\frac{\omega_b}{c_f} i_{o,d} + \frac{\omega_b}{c_f} i_{l,d} + \omega_b \omega_g v_{o,q}$

4) $s \cdot v_{o,q} = -\frac{\omega_b}{c_f} i_{o,q} + \frac{\omega_b}{c_f} i_{l,q} - \omega_b \omega_g v_{o,d}$

5) $s \cdot i_{o,d} = -\frac{i_{o,d} r_g \omega_b - v_{o,d} \omega_b + v_{n,d} \omega_b \cos\left(\delta\theta_{VSM} + k_{ff\delta} k_3\right) + v_{n,q} \omega_b \sin\left(\delta\theta_{VSM} + k_{ff\delta} k_3\right)}{l_g} + i_{o,q} \omega_b \omega_g$

6) $s \cdot i_{o,q} = -\frac{i_{o,q} r_g \omega_b - v_{o,q} \omega_b + v_{n,q} \omega_b \cos\left(\delta\theta_{VSM} + k_{ff\delta} k_3\right) - v_{n,d} \omega_b \sin\left(\delta\theta_{VSM} + k_{ff\delta} k_3\right)}{l_g} - i_{o,d} \omega_b \omega_g$

7) $s \cdot \gamma_d = -i_{ld} - \frac{r_s v_{om,d} + k_q r_s \left(q_m - q^*\right) - r_s \hat{v}^* + \omega_{VSM} l_s v_{om,q}}{r_s^2 + l_s^2 \omega_{VSM}^2}$

8) $s \cdot \gamma_q = -i_{lq} - \frac{r_s v_{om,q} - k_q \omega_{VSM} l_s \left(q_m - q^*\right) - \omega_{VSM} l_s \left(v_{om,d} - \hat{v}^*\right)}{r_s^2 + l_s^2 \omega_{VSM}^2}$

9) $s \cdot \phi_d = \omega_{ad} \left(v_{o,d} - \phi_d\right)$

10) $s \cdot \phi_q = \omega_{ad} \left(v_{o,q} - \phi_q\right)$

11) $s \cdot q_m = \omega_{qf} \left(-q_m - i_{o,q} v_{o,d} + i_{o,d} v_{o,q}\right)$

12) $s \cdot \omega_{VSM} = \frac{z_1}{T_a T_1 T_2 T_3} - \frac{k_d \left(\omega_{VSM} - \omega_n - k_{i,PLL} \varepsilon_{PLL} - k_{p,PLL} \arctan \frac{v_{PLL,q}}{v_{PLL,d}} \right) + i_{o,d} v_{o,d} + i_{o,q} v_{o,q} + k_\omega \left(\omega_{VSM} - \omega_{VSM}^*\right)}{T_a}$

13) $s \cdot \delta\theta_{VSM} = -\omega_b (\omega_g - \omega_{VSM})$

14) $s \cdot v_{om,d} = \omega_{vo} \left(v_{o,d} - v_{om,d}\right)$

15) $s \cdot v_{om,q} = \omega_{vo} \left(v_{o,q} - v_{om,q}\right)$

16) $s \cdot v_{PLL,d} = -v_{PLL,d} \omega_{lpPLL} + v_{o,d} \omega_{lpPLL} \cos\left(\delta\theta_{PLL} - \delta\theta_{VSM} - k_{ff\delta} k_3\right) + v_{oq} \omega_{lpPLL} \sin\left(\delta\theta_{PLL} - \delta\theta_{VSM} - k_{ff\delta} k_3\right)$

17) $s \cdot v_{PLL,q} = -v_{PLL,q} \omega_{lpPLL} + v_{o,q} \omega_{lpPLL} \cos\left(\delta\theta_{PLL} - \delta\theta_{VSM} - k_{ff\delta} k_3\right) - v_{od} \omega_{lpPLL} \sin\left(\delta\theta_{PLL} - \delta\theta_{VSM} - k_{ff\delta} k_3\right)$

18) $s \cdot \varepsilon_{PLL} = \arctan \frac{v_{PLL,q}}{v_{PLL,d}}$,

19) $s \cdot \delta\theta_{PLL} = \omega_b \left(-\omega_g + \omega_n + k_{p,PLL} \arctan \frac{v_{PLL,q}}{v_{PLL,d}} + k_{i,PLL} \varepsilon_{PLL} \right)$

20) $s \cdot z_1 = z_2$

21) $s \cdot z_2 = z_3$

22) $s \cdot z_3 = -\frac{\left(1 - p^* T_1 T_2 T_3\right)}{T_1 T_2 T_3} z_1 - \frac{\left(T_1 + T_2 + T_3\right)}{T_1 T_2 T_3} z_2 - \frac{\left(T_1 T_2 + T_1 T_3 + T_2 T_3\right)}{T_1 T_2 T_3} z_3$

Salvatore D'Arco received the M.Sc. and Ph.D. degrees in electrical engineering from the University of Naples "Federico II," Naples, Italy, in 2002 and 2005, respectively.

From 2006 to 2007, he was a postdoctoral researcher at the University of South Carolina, Columbia, SC, USA. In 2008, he joined ASML, Veldhoven, the Netherlands, as a Power Electronics Designer, where he worked until 2010. From 2010 to 2012, he was a postdoctoral researcher in the Department of Electric Power Engineering at the Norwegian University of Science and Technology (NTNU), Trondheim, Norway. In 2012, he joined SINTEF Energy Research where he currently works as a Chief Research Scientist. He is the author of more than 100 scientific papers and is the holder of one patent. His main research activities are related to control and analysis of power-electronic conversion systems for power system applications, including real-time simulation and rapid prototyping of converter control systems.

Jon Are Suul (M'11) received the M.Sc. degree in energy and environmental engineering and the Ph.D. degree in electric power engineering from the Norwegian University of Science and Technology (NTNU), Trondheim, Norway, in 2006 and 2012, respectively.

From 2006 to 2007, he was with SINTEF Energy Research, Trondheim, where he was working with simulation of power electronic converters and marine propulsion systems until starting his Ph.D. studies. Since 2012, he has been a Research Scientist with SINTEF Energy Research, first in a part-time position while working as a part-time Postdoctoral Researcher with the Department of Electric Power Engineering of NTNU until 2016. Since August 2017, he has been an Adjunct Associate Professor with the Department of Engineering Cybernetics, NTNU. His research interests are mainly related to modelling, analysis, and control of power electronic converters in power systems, renewable energy applications, and electrification of transport.

Dr. Suul is an Editor of the IEEE Journal of Emerging and Selected Topics in Power Electronics, and an Associate Editor of the IEEE Transactions on Energy Conversion.